Tailoring of the photocatalytic activity of CeO_2 nanoparticles by the presence of plasmonic Ag nanoparticles

Shuang Zhao[1], Marc Riedel[2], Javier Patarroyo[3], Neus G. Bastús[3], Victor Puntes[3,4,5], Zhao Yue[6*], Fred Lisdat[2*], Wolfgang J. Parak[1*]

[1] Fachbereich Physik, CHyN, Universität Hamburg, 22761 Hamburg, Germany.
[2] Biosystems Technology, Institute of Life Sciences and Biomedical Technologies, Technical University of Applied Sciences Wildau, 15745 Wildau, Germany.
[3] Institut Català de Nanociència i Nanotecnologia (ICN2), CSIC and BIST, Campus UAB, Bellaterra, 08193 Barcelona, Catalonia, Spain.
[4] Vall d'Hebron Institut de Recerca (VHIR), 08035 Barcelona, Catalonia, Spain
[5] ICREA, Pg. Lluís Companys 23, 08010 Barcelona, Catalonia, Spain.
[6] Department of Microelectronics, Nankai University, 30071 Tianjin, China.
[*] corresponding authors: yuezhao@nankai.edu.cn, flisdat@th-wildau.de, wolfgang.parak@uni-hamburg.de

SUPPORTING INFORMATION

I) Additional nanoparticle characterization

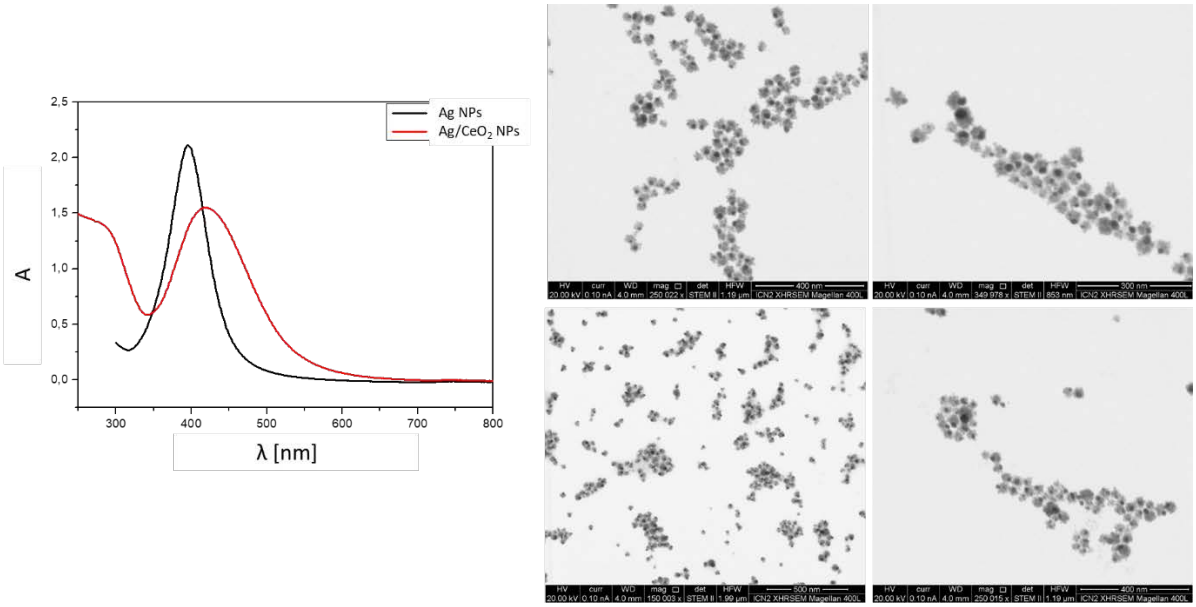

Figure S1. Additional UV/vis absorption spectra of the Ag NPs and the Ag/CeO_2 NPs, as well as additional TEM images of the Ag/CeO_2 NPs.

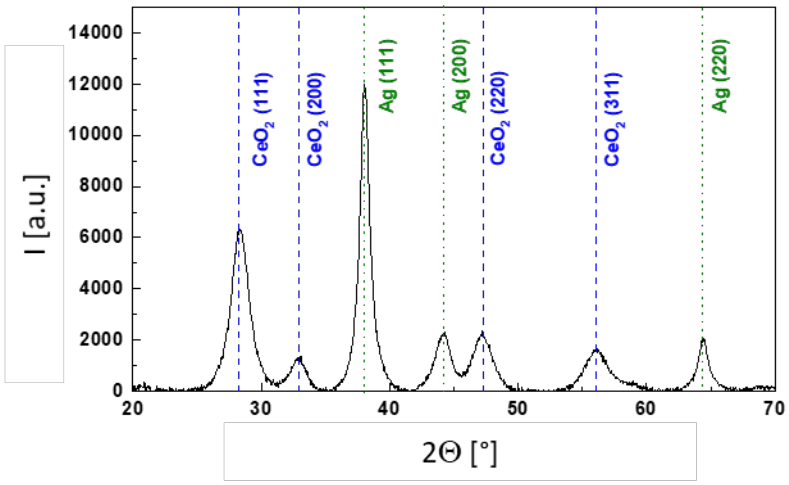

Figure S2. XRD scattering intensity I(2Θ) of Ag/CeO_2 NPs. The lines show the scattering peaks of CeO_2 (JCPDS 34–0394, in blue) and of the cubic phase of Ag (JCPDS 04-0783, in green) from the JCPDS-International Centre for Diffraction Data database.

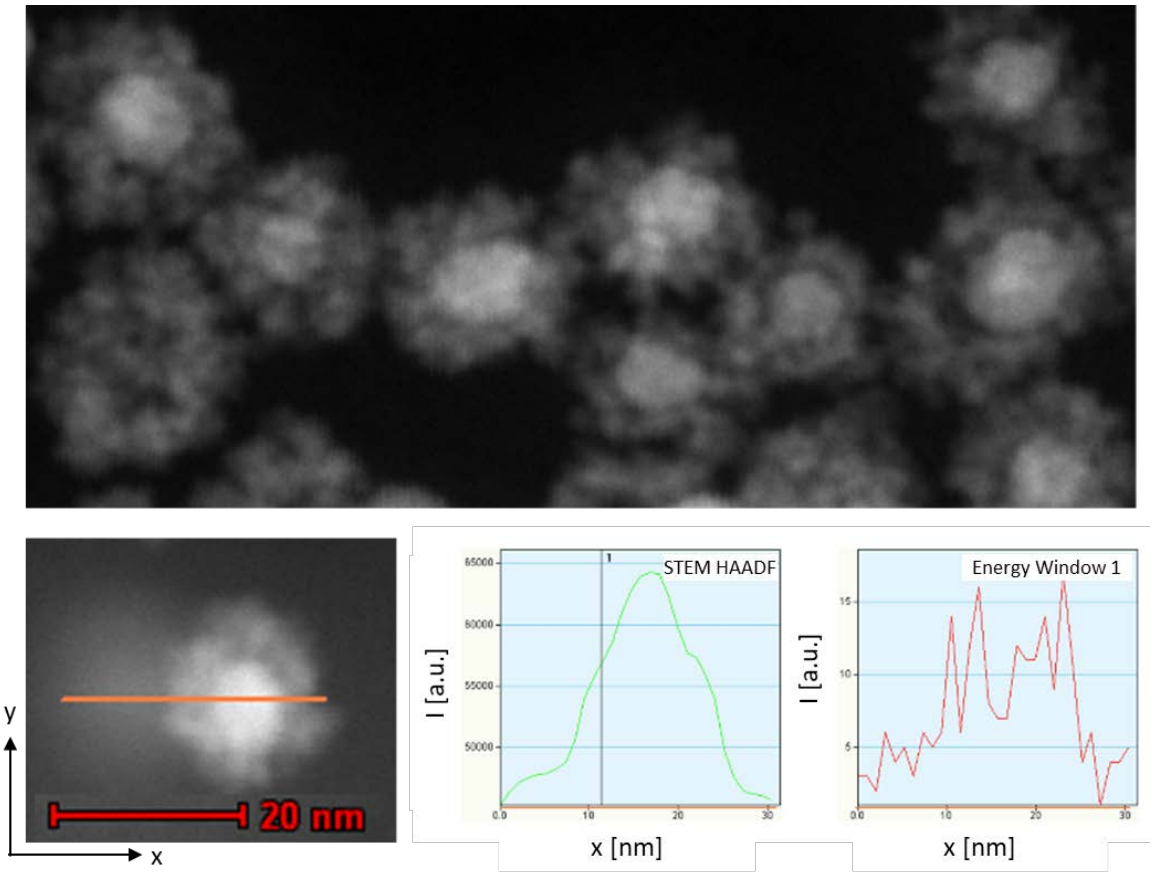

Figure S3. Advanced characterization of the Ag/CeO_2 hybrid NPs. (top) General high-angle annular dark-field scanning transmission electron microscopy (HAADF STEM) image. (bottom) energy-dispersive X-ray spectroscopy (EDS) line scanning profile of the Ag/CeO_2 hybrid NPs indicated in the HAADF STEM image.

II) Surface coverage of nanoparticles on gold electrodes

Fabrication of working electrodes

Single layer coatings: Gold electrodes (Suzhou Research Materials Microtech Co. Ltd, China) were used as working electrodes (WEs) of the three-system, similar to our previous publication [1]. The gold electrodes were first processed by soft ultrasonic cleaning in acetone, water, and alcohol for 7 min each. N_2 was used to dry the electrodes after each cleaning step. In a next step the gold electrodes were incubated in 0.1 M aqueous cysteamine solution for 1 hour in the dark, which chemisorbed and rendered the surface of the gold electrode positively charged. This was followed by further 12 hours incubation in the water to remove unbound cysteamine from the working electrode. After drying with N_2, the prepared gold/cysteamine electrodes were incubated in the solution of negatively charged nanoparticles (NPs) for 12 hours to form a single layer of NPs, leading to gold/cysteamine/NP electrodes (for all systems used: CeO_2 NPs, hybrid Ag/CeO_2 NPs and mixtures of Ag NPs (with negatively charged citrate ligand) and CeO_2 NPs).

Multilayer coatings: The gold/cysteamine/NP electrodes as described in the single layer coating description were used to build multilayer structures. Here, a positively charged polyelectrolyte poly(diallyldimethylammonium chloride; PDDA 10% in water) was used as intermittent layer between the different NP layers. As the NPs are negatively charged, the gold/cysteamine/NP electrode surface charge is negative. To render the surface charge again positive for the adsorption of the next negatively charged NP layer, the gold/cysteamine/NP electrode was incubated first in the PDDA solution for 30 min, followed by thorough washing with water and drying with N_2. The positively charged gold/cysteamine/NP/PDDA electrode was then incubated in NP solution for 12 hours to immobilize the next layer of NPs. The PDDA and NP coating steps were repeated n times to build a multilayer structure as gold/cysteamine/NP/$[PDDA/NP]_n$.

ICP-MS analysis of the NPs immobilized on the Au electrodes: The working electrodes were dissolved in aqua regia for 24 h (e.g. the NPs and the Au layer of the working electrodes were dissolved) and the ion contents were determined with inductively coupled plasma mass spectrometry (ICP-MS). A sketch is shown in Figure S4. Note that this way of determining the NP coverage on top of the electrodes is different than the one used in a previous study [1]. The masses of Au, Ag, and Ce as detected per WE were $m_{Au/W}E$, $m_{Ag/WE}$, and $m_{Ce/WE}$, respectively.

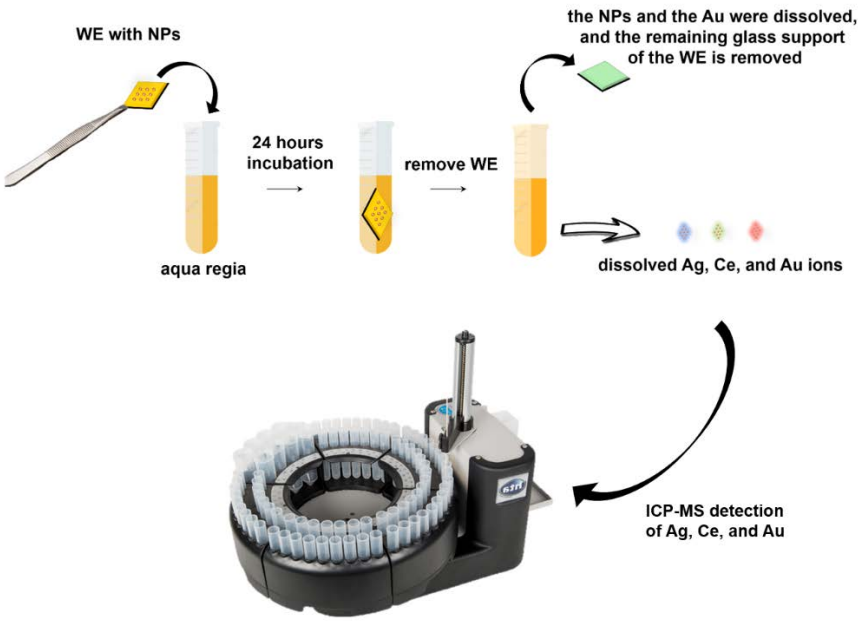

Figure S4. Sketch for the determination of NP coverage of the working electrodes.

The detected amount of Au was used as internal control. The area of the working electrodes is A_{WE} = 1 cm^2. According to the manufacturer the thickness of the Au film on the glass support of the WEs is d_{WE} = 200 nm. This results in a mass of Au per WE of $m_{Au/WE} = A_{WE} \cdot d_{WE} \cdot \rho_{Au}$ = 0.39 mg, using the bulk density of Au of ρ_{Au} = 19.32 g/cm^3. In Figure S5 the mass of Au per WE as determined with ICP-MS is shown for several WEs, and shows a good match with the expected value.

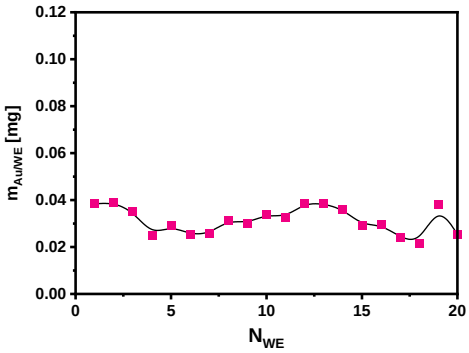

Figure S5. Mass of Au per working electrode $m_{Au/WE}$ as determined for different WEs (N_{WE} = number of the working electrode which was analyzed).

To determine the number of NPs per WE from the determined Ce and Ag concentrations first the masses of Ce and Ag per NP were estimated.

The mass of one CeO_2 NP is $m_c(CeO_2\ NP) = V_c(CeO_2\ NP) \cdot \rho(CeO_2) = (4/3) \cdot \pi \cdot (d_c(CeO_2\ NP)/2)^3 \cdot \rho(CeO_2) \approx 13.79 \cdot 10^{-18}$ g, using the bulk density of CeO_2 of $\rho(CeO_2)$ = 7.22 g/cm^3. V_c is the volume of one NP core and d_c the core diameter as determined by transmission electron microscopy (TEM) of $d_c(CeO_2\ NP)$ = 15.4 nm. CeO_2 NPs contain two oxygen (molar mass M_O =

16 g/mol) atoms per cerium atom (molar mass M_{Ce} = 140 g/mol). The mass of cerium of one CeO_2 NP thus is $m_{c,Ce}(CeO_2\ NP) = (M_{Ce}/(2\cdot M_O+M_{Ce}))\cdot m_c(CeO_2\ NP) \approx 1.12\cdot10^{-17}$ g.

The mass of Ag in one Ag NP is $m_c(Ag\ NP) = (4/3)\cdot\pi\cdot(d_c(Ag\ NP)/2)^3\cdot\rho(Ag) \approx 1.07\cdot10^{-18}$ g, using the bulk density of Ag of $\rho(Ag) = 10.49\ g/cm^3$ and $d_c(Ag\ NP) = 5.8$ nm as determined by TEM.

For the mass calculation of the hybrid Ag/CeO_2 core/shell NPs those were assumed to be Ag spheres with diameter $d_c(Ag\ NP)$ surrounded by a CeO_2 shell with thickness of $(d_c(Ag/CeO_2\ NP) - d_c(Ag\ NP))/2$. This is obviously an approximation with large error, as the CeO_2 part around the Ag cores is not homogeneous, see Figure 1c. The mass of Ag in one hybrid Ag/CeO_2 core/shell NP thus is $m_{c,Ag}(Ag/CeO_2\ NP) = (4/3)\cdot\pi\cdot(d_c(Ag\ NP)/2)^3 \approx 2.6\cdot10^{-18}$ g. The mass of Ce in one hybrid Ag/CeO_2 core/shell NP is $m_{c,Ce}(Ag/CeO_2\ NP) = (M_{Ce}/(2\cdot M_O+M_{Ce}))\cdot((4/3)\cdot\pi\cdot(d_c(Ag/CeO_2\ NP)/2)^3 - (4/3)\cdot\pi\cdot(d_c(Ag\ NP)/2)^3)\cdot\rho(CeO_2) \approx 13.11\cdot10^{-18}$ g. Hereby the TEM values $d_c(Ag/CeO_2\ NP) = 15.8$ nm and $d_c(Ag\ NP) = 7.8$ nm were used.

Based on the determined masses of Ag and Ce per WE, the number of NPs per WE area A_{WE} can be determined as follows:

1) CeO_2 NPs: $n(CeO_2\ NP) = (m_{Ce/WE}/m_{c,Ce}(CeO_2\ NP))/A_{WE}$;

N_{WE}	$m_{Ce/WE}$ [g]	$m_{c,Ce}(CeO_2\ NP)$ [g]	A_{WE} [cm^2]	$n(CeO_2\ NP)$ [cm^{-2}]
1	$0.59\cdot10^{-6}$	$1.12\cdot10^{-17}$	1	$0.53\cdot10^{11}$
2	$0.62\cdot10^{-6}$	$1.12\cdot10^{-17}$	1	$0.55\cdot10^{11}$
3	$0.59\cdot10^{-6}$	$1.12\cdot10^{-17}$	1	$0.53\cdot10^{11}$
4	$0.60\cdot10^{-6}$	$1.12\cdot10^{-17}$	1	$0.54\cdot10^{11}$
5	$0.66\cdot10^{-6}$	$1.12\cdot10^{-17}$	1	$0.59\cdot10^{11}$
Average	$0.61\cdot10^{-6}$	$1.12\cdot10^{-17}$	1	$0.55\cdot10^{11}$

2) Ag NPs: $n(Ag\ NP) = (m_{Ag/WE}/m_c(Ag\ NP))/A_{WE}$;

N_{WE}	$m_{Ag/WE}$ [g]	$m_{c,Ag}(Ag\ NP)$ [g]	A_{WE} [cm^2]	$n(Ag\ NP)$ [cm^{-2}]
1	$0.63\cdot10^{-7}$	$1.07\cdot10^{-18}$	1	$0.59\cdot10^{11}$
2	$0.66\cdot10^{-7}$	$1.07\cdot10^{-18}$	1	$0.62\cdot10^{11}$
3	$0.58\cdot10^{-7}$	$1.07\cdot10^{-18}$	1	$0.54\cdot10^{11}$
4	$0.64\cdot10^{-7}$	$1.07\cdot10^{-18}$	1	$0.60\cdot10^{11}$
5	$0.67\cdot10^{-7}$	$1.07\cdot10^{-18}$	1	$0.63\cdot10^{11}$
Average	$0.64\cdot10^{-7}$	$1.07\cdot10^{-18}$	1	$0.60\cdot10^{11}$

3) Hybrid Ag/CeO_2 NPs: $n(Ag/CeO_2\ NP) = (m_{Ag/WE}/m_{c,Ag}(Ag/CeO_2\ NP))/A_{WE}$ or $n(Ag/CeO_2\ NP) = (m_{Ce/WE}/m_{c,Ce}(Ag/CeO_2\ NP))/A_{WE}$.

N_{WE}	$m_{Ag/WE}$ [g]	$m_{c,Ag}(Ag/CeO_2\ NP)$ [g]	A_{WE} [cm^2]	$n(Ag/CeO_2\ NP)$ [cm^{-2}]
1	$1.06\cdot10^{-7}$	$2.6\cdot10^{-18}$	1	$0.41\cdot10^{11}$
2	$1.14\cdot10^{-7}$	$2.6\cdot10^{-18}$	1	$0.44\cdot10^{11}$
3	$1.14\cdot10^{-7}$	$2.6\cdot10^{-18}$	1	$0.44\cdot10^{11}$
4	$1.12\cdot10^{-7}$	$2.6\cdot10^{-18}$	1	$0.43\cdot10^{11}$
5	$1.05\cdot10^{-7}$	$2.6\cdot10^{-18}$	1	$0.40\cdot10^{11}$
Average	$1.10\cdot10^{-7}$	$2.6\cdot10^{-18}$	1	$0.42\cdot10^{11}$

N_{WE}	$m_{Ce/WE}$ [g]	$m_{c,Ce}(Ag/CeO_2\ NP)$ [g]	A_{WE} [cm^2]	$n(Ag/CeO_2\ NP)$ [cm^{-2}]
1	$0.54\cdot10^{-6}$	$13.11\cdot10^{-18}$	1	$0.41\cdot10^{11}$
2	$0.58\cdot10^{-6}$	$13.11\cdot10^{-18}$	1	$0.44\cdot10^{11}$
3	$0.58\cdot10^{-6}$	$13.11\cdot10^{-18}$	1	$0.44\cdot10^{11}$
4	$0.59\cdot10^{-6}$	$13.11\cdot10^{-18}$	1	$0.45\cdot10^{11}$
5	$0.55\cdot10^{-6}$	$13.11\cdot10^{-18}$	1	$0.42\cdot10^{11}$
Average	$0.57\cdot10^{-6}$	$13.11\cdot10^{-18}$	1	$0.43\cdot10^{11}$

For the hybrid Ag/CeO_2 core/shell NPs the comparison of calculating $n(Ag/CeO_2\ NP)$ either from the Ce or the Ag determination is an internal control for the validity of our calculations and in fact there is a reasonable agreement.

In order to determine the percentage of surface coverage the cross-section are of the CeO_2 NPs (the cross-section of one single NP is: $A_c(CeO_2\ NP) = \pi\cdot(d_c(CeO_2\ NP)/2)^2$) is divided by the area of the working electrode. The total number of NPs on the WE is: $n(CeO_2\ NP)\cdot A_{WE}$. The percentage of surface coverage thus is $A_c(CeO_2\ NP)\cdot n(CeO_2\ NP)\cdot A_{WE}/A_{WE}\cdot100\% = A_c(CeO_2\ NP)\cdot n(CeO_2\ NP)\cdot100\% \approx 10.2\ \%$. Similar to that, the percentage of surface coverage for Ag NPs and hybrid Ag/CeO_2 core/shell NPs are 1.6% and 8.5%, respectively.

In Figure S6 the surface coverage of CeO_2 NPs on top of different working electrodes which have been coated with mixtures of CeO_2 NPs and Ag NPs is shown.

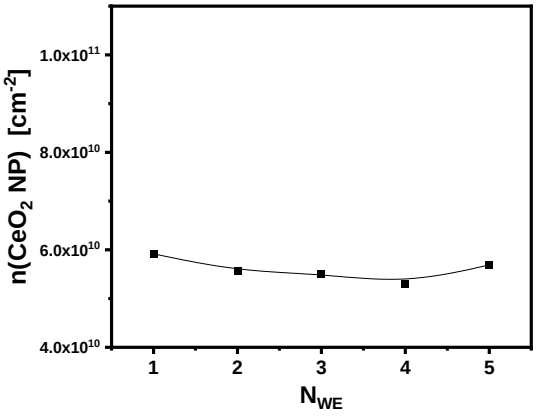

Figure S6. The number of CeO_2 NPs per area from the electrodes immobilized with a single layer of mixtures of CeO_2 NPs and Ag NPs as discussed in Figure 3c with Ag (-) NPs with d_c = 5.8 $\pm$ 0.4 nm.

In Figure S7 the surface coverage of mixtures of Ag NPs with different diameter and CeO_2 NPs on top of working electrodes is shown. In Figure S8 the difference between Ag (-) NPs and Ag (+) NPs and in Figure S9 the coverage for different mixtures of Ag NPs and CeO_2 NPs is shown. Finally, in Figure S11 the surface coverage for multilayers is provided.

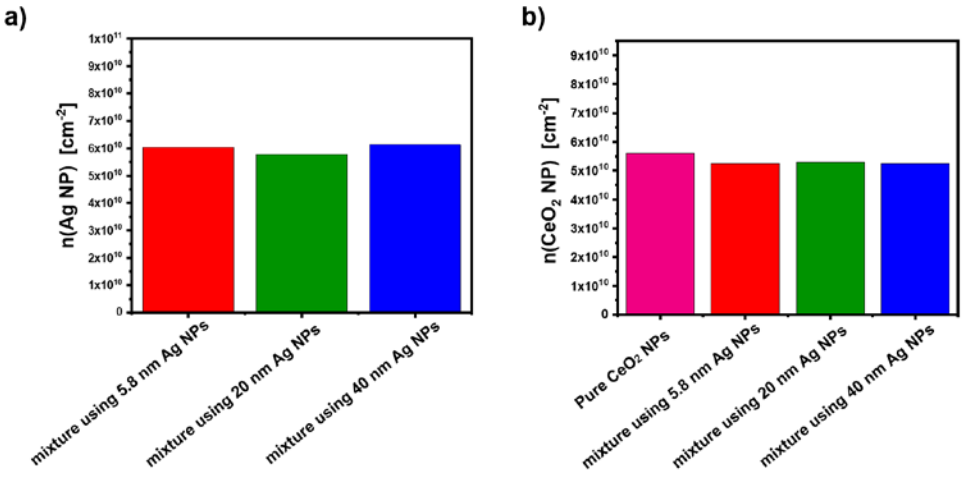

Figure S7. (a) Coverage of Ag NPs in single layers of mixtures of Ag (-) NPs of different diameter and CeO_2 NPs. (b) Corresponding coverage of CeO_2 NPs. These data correspond to the measurements shown in Figure 3c.

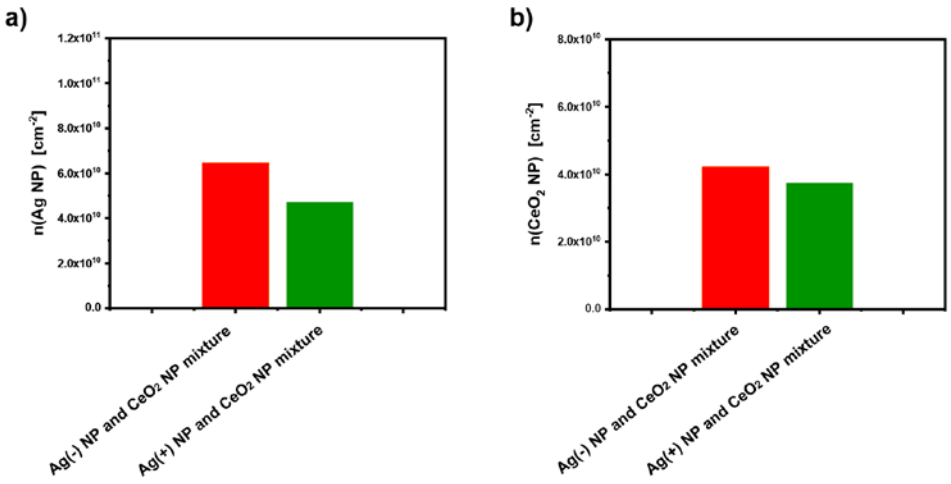

Figure S8. (a) Coverage of Ag NPs in single layers of mixtures of Ag (-) NPs or Ag (+) NPs and CeO_2 NPs. (b) Corresponding coverage of CeO_2 NPs for the mixtures. These data correspond to the measurements shown in Figure 4.

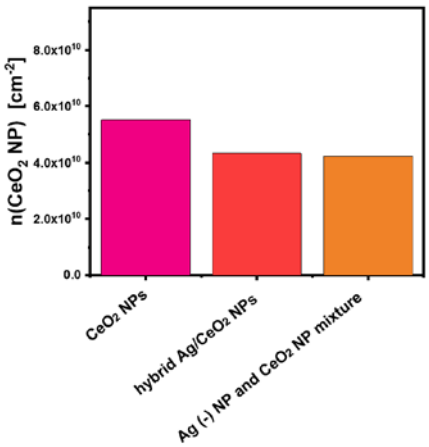

Figure S9. Coverage of CeO_2 NPs in single layers of pure CeO_2 NPs, hybrid Ag/CeO_2 NPs, and mixtures of Ag (-) NPs and CeO_2 NPs. These data correspond to the measurements shown in Figure 4.

The WEs remained stable against photo-oxidation. The WEs with single layers of CeO_2 NP and Ag (-) NP (d_c = 5.8 nm) mixtures and the hybrid Ag/CeO_2 NPs (cf. Figure 4) were put under 30 min white light illumination in phosphate buffered saline (PBS) and after illumination the amount of released Ag NPs from the immobilized Ag NPs was detected with ICP-MS. The released Ag was converted in a virtual number of Ag NPs per WE and is shown in Figure S10. Comparison of the released amount (Figure S10) with the original Ag NP amount (Figure S8) shows that in case of Ag NP /CeO_2 NP mixtures parts of the Ag NPs in fact dissolve (up to 46%). However, in case of the hybrid Ag/CeO_2 NPs the Ag NP part remains largely intact, most likely

due to protection of the Ag cores by the CeO_2 shells and/or a better interaction of these NPs with the modified surface.

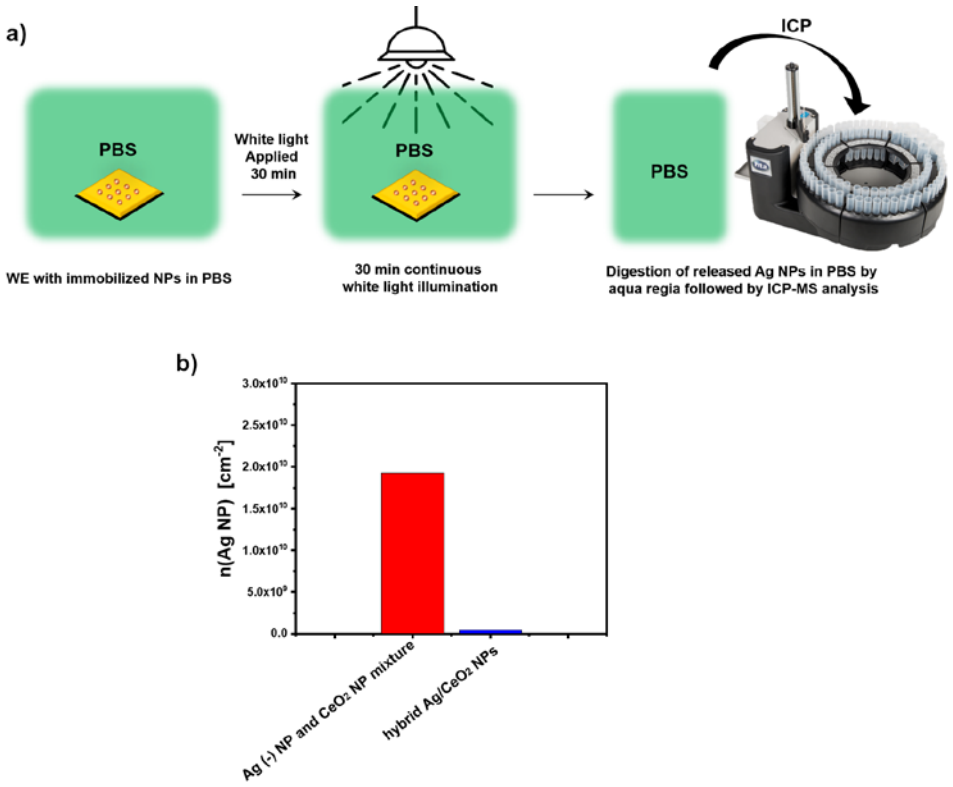

Figure S10. (a) Sketch for the photo-corrosion measurement. (b) The dissolved Ag NPs are converted into a virtual Ag NP coverage n(Ag NP). The percentage of release Ag ions is the ratio of the released Ag NPs n(Ag NP) from Figure S10 to the amount of original Ag NPs n(Ag NP) from Figure S8.

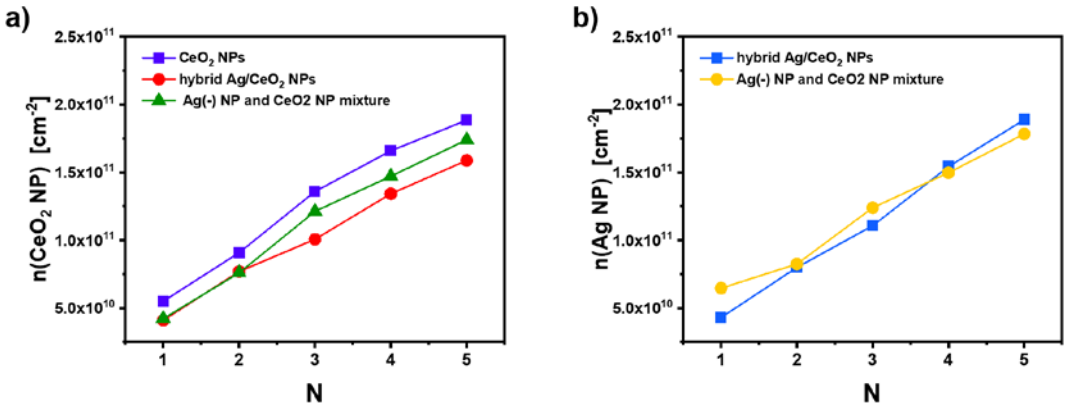

Figure S11. Coverage of (a) CeO_2 NPs and (b) Ag NPs in multilayers (N = layer number) of pure CeO_2 NPs, hybrid Ag/CeO_2 NPs, and mixtures of Ag (-) NPs and CeO_2 NPs. These data correspond to the measurements shown in Figure 5.

III) Additional photocurrent measurements

Here experiments are collected which illustrate the defined photocurrent behavior at different electrode bias (cf. Figure S12). Furthermore, the stability of the photocurrent behavior has been analyzed in a short term range for the arrangements of a single NP layer (cf. Figure S13) and NP multilayers (cf. Figure S14), which illustrates the beneficial application of hybrid NPs from another point of view.

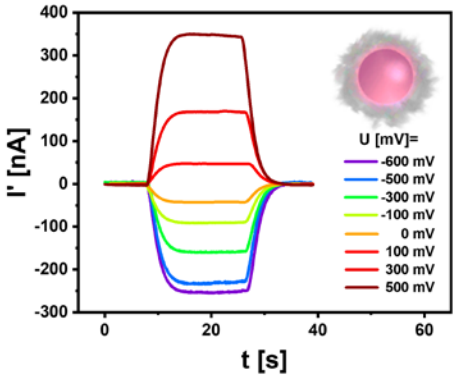

Figure S12. Chopped photocurrent I' in dependence of the bias voltage U versus Ag/AgCl for a single layer of hybrid Ag/CeO_2 NPs. The amplitude of the photocurrent I versus U is plotted in Figure S7.

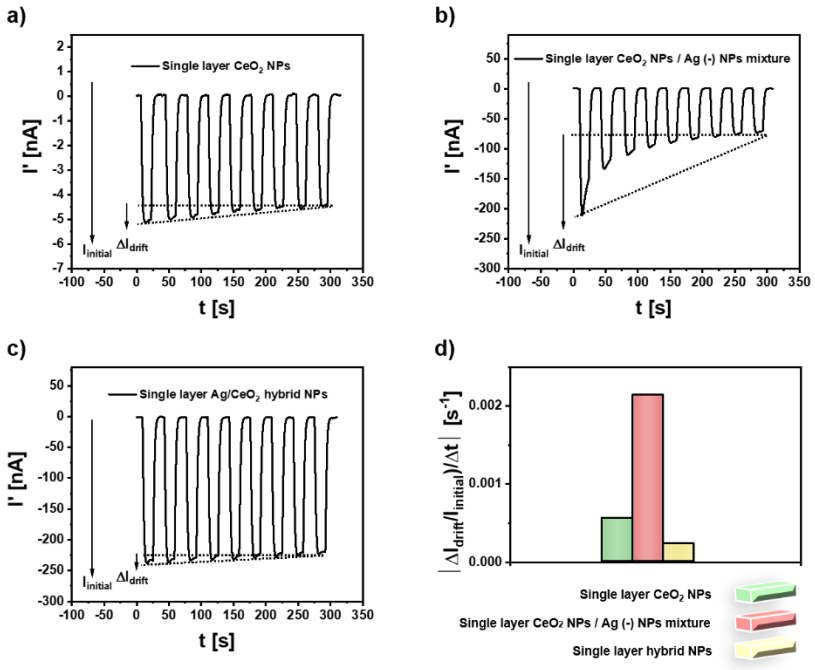

Figure S13. The time dependence of the chopped photocurrent I' as recorded on a single layer of (a) CeO_2 NPs, (b) a mixture of CeO_2 NPs and Ag (-) NPs, and (c) hybrid Ag/CeO_2 NPs at U = -500 mV versus an Ag/AgCl reference electrode in 0.1 M PBS (pH=7.4) under chopped white light illumination. The change in photocurrent amplitude ΔI_{drift} over the initial amplitude was determined in order to characterize drift [2]. (d) Percentage of drift for the 3 different configurations.

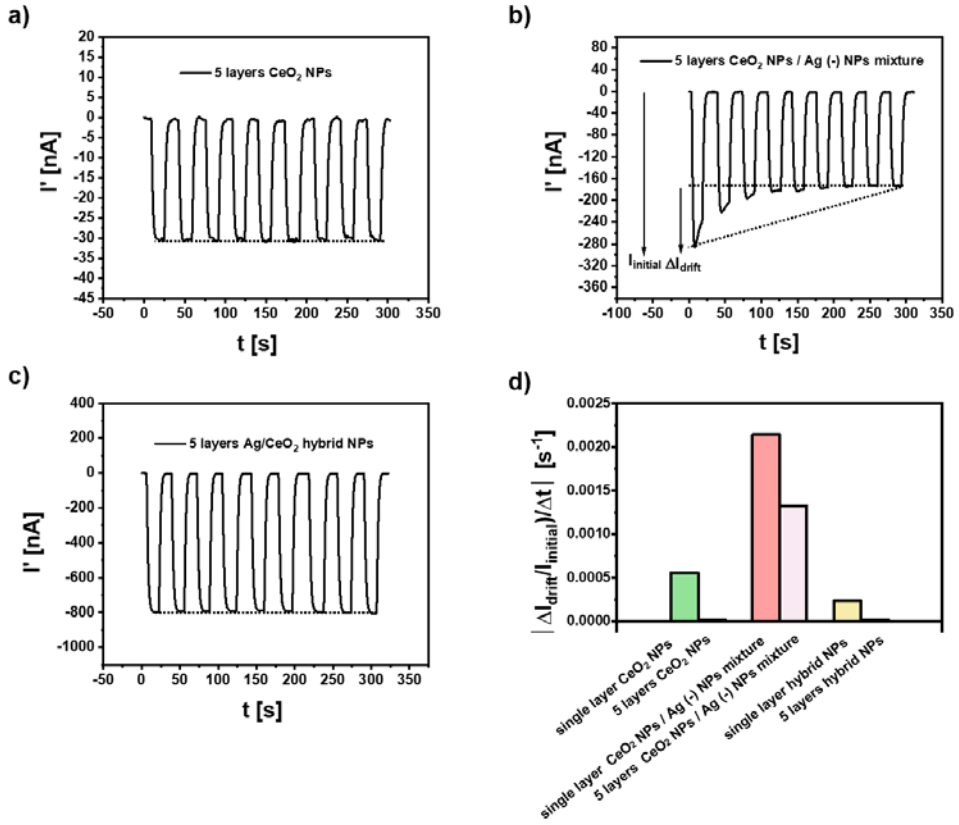

Figure S14. The time dependence of the chopped photocurrent I' as recorded on a multilayer (N = 5) of (a) CeO_2 NPs, (b) a mixture of CeO_2 NPs and Ag (-) NPs, and (c) hybrid Ag/CeO_2 NPs at U = -500 mV versus an Ag/AgCl reference electrode in 0.1 M PBS (pH=7.4) under chopped white light illumination. The change in photocurrent amplitude ΔI_{drift} over the initial amplitude was determined in order to characterize drift [2]. (d) Percentage of drift for the 3 different configurations.

IV) Numbers for the sketch of the band levels

First, the situation at CeO_2 NPs without Ag NPs are considered (Figure 7a). We assume that without external bias the energy level of the Au working electrode aligns with the fermi level (E_F) of the CeO_2 NPs, which (without considering potential surface states and doping impurities) would lie between the energy levels of the valence (E_{VB}) and conduction band (E_{CB}). Approximated by its absorption peak from Figure 2 the band gap of the CeO_2 NPs is $E_g(CeO_2) = h \cdot c/\lambda = 4.1 \cdot 10^{-15}$ eV·s $\cdot 3 \cdot 10^8$ m·s^{-1} /$270 \cdot 10^{-9}$ m ≈ 4.6 eV. We align the energy level of the redox reaction at the CeO_2 surface with the Fermi level of CeO_2. A plausible reduction reaction at the CeO_2 surface is $H_2O_2 + 2H^+ + 2e^- \rightarrow 2\ H_2O$. The standard electrode potential (e.g. versus the potential of the standard hydrogen electrode) of this reaction at pH = 7 is $U'_{H2O2/H2O} \approx 1.36$ V. This corresponds to an energy level E' = -e·U', in reference to the energy of the standard hydrogen electrode. The standard electrode potential of the Ag/AgCl electrode (versus the normal hydrogen electrode; 1 M KCl concentration) is $U'_{Ag/AgCl} \approx 0.2$ V. By using this value the potential of the hydrogen peroxide reaction can be referred to the potential of the Ag/AgCl electrode as $U_{H2O2/H2O} = U'_{H2O2/H2O} - U'_{Ag/AgCl}$. The Ag/AgCl electrode is set by the potentiostat to ground level and referred to this level the potential of the working electrode is the bias U. In Figure 7a in the main manuscript the bias is set to U = -0.5 V.

V) References

1. S. Zhao, M. Riedel, J. Patarroyo, N. Bastus, V. Puntes, Z. Yue, F. Lisdat and W. J. Parak, *Nanoscale*, 2021, **13**, 980-990.
2. Z. Yue, W. Khalid, M. Zanella, A. Z. Abbasi, A. Pfreundt, P. Rivera_Gil, K. Schubert, F. Lisdat and W. J. Parak, *Analytical and Bioanalytical Chemistry*, 2010, **396**, 1095-1103.